Cyanobacterial Growth on Municipal Wastewater Requires Low Temperatures

Travis C. Korosh[a,b], Andrew Dutcher[c], Brian F. Pfleger [a,d,], and Katherine D. McMahon [c,e] *

[a] Department of Chemical and Biological Engineering, University of Wisconsin-Madison, Madison, WI 53706, United States
[b] Environmental Chemistry and Technology Program, University of Wisconsin-Madison, Madison, WI 53706, United States
[c] Department of Civil and Environmental Engineering, University of Wisconsin-Madison, Madison, WI 53706, United States
[d] Microbiology Doctoral Training Program, University of Wisconsin-Madison, Madison, WI 53706, United States
[e] Department of Bacteriology, University of Wisconsin-Madison, Madison, WI 53706, United States

* Corresponding author. 5552 Microbial Science Building, 1550 Linden Drive, Madison, WI 53706, United States. Phone: +1 608 890 2836. Fax: +1 608 262-9865. E-mail address: trina.mcmahon@wisc.edu.

Keywords: Nutrient removal, cyanobacteria, Synechococcus strain PCC 7002

ABSTRACT

Side-streams in wastewater treatment plants can serve as concentrated sources of nutrients (i.e. nitrogen and phosphorus) to support the growth of photosynthetic organisms that ultimately serve as feedstock for production of fuels and chemicals. However, other chemical characteristics of these streams may inhibit growth in unanticipated ways. Here, we evaluated the use of liquid recovered from municipal anaerobic digesters via gravity belt filtration as a nutrient source for growing the cyanobacterium *Synechococcus* sp. strain PCC 7002. The gravity belt filtrate (GBF) contained high levels of complex dissolved organic matter (DOM), which seemed to negatively influence cells. We investigated the impact of GBF on physiological parameters such as growth rate, membrane integrity, membrane composition, photosystem composition, and oxygen evolution from photosystem II. At 37°C, we observed an inverse correlation between GBF concentration and membrane integrity. Radical production was also detected upon exposure to GBF at 37°C. However, at 27°C the dose dependent relationship between GBF concentration and lack of membrane integrity was abolished. Immediate resuspension of strains in high doses of GBF showed markedly reduced oxygen evolution rates relative to the control. Together, this suggests that one mechanism responsible for GBF toxicity to *Synechococcus* is the interruption of photosynthetic electron flow and subsequent phenomena. We hypothesize this is likely due to the presence of phenolic compounds within the DOM.

IMPORTANCE

Cyanobacteria are viewed as promising platforms to produce fuels and/or high-value chemicals as part of so-called “bio-refineries”. Their integration into wastewater treatment systems is particularly interesting because removal of the nitrogen and phosphorus in many wastewater

51 streams is an expensive but necessary part of wastewater treatment. In this study, we evaluated
52 strategies for cultivating *Synechococcus* strain PCC 7002 on media comprised of two wastewater
53 streams; treated secondary effluent supplemented with the liquid fraction extracted from sludge
54 following anaerobic digestion. This strain is commonly used for metabolic engineering to produce
55 a variety of valuable chemical products and product precursors (e.g. lactate). However, initial
56 attempts to grow PCC 7002 under otherwise standard conditions of light and temperature failed.
57 We thus systematically evaluated alternative cultivation conditions and then used multiple
58 methods to dissect the apparent toxicity of the media under standard cultivation conditions.
59
60

61 **INTRODUCTION**

62 The need to develop non-petroleum based platforms for fuel and chemical production is
63 driving researchers to explore alternatives that harness renewable energy sources while minimizing
64 other environmental impacts such as freshwater depletion, eutrophication, and the use of arable
65 land for non-food production. Cyanobacteria are particularly attractive such platforms due to their
66 genetic tractability, rapid growth rates, halotolerance, and ability to be grown on non-productive
67 land with simple nutrient requirements (1, 2). According to published life cycle assessments, a
68 large portion of the associated costs of culturing photoautotrophs are tied to upstream costs, such
69 as CO_2 delivery and fertilizer application (3). High phosphorus/nitrogen removal rates and energy
70 efficiencies have been reported for photobioreactor and open pond cultivation systems using
71 wastewater streams rich in nitrogen and phosphorus (4, 5). Therefore, it may be possible to offset
72 the requirement for fertilizer by reclaiming nutrients from wastewater. This approach could yield
73 the sought-after non-petroleum based alternative while also providing a more effective means of
74 nutrient and metal removal than conventional wastewater treatment (6–8). Side-streams from
75 common wastewater treatment facilities such as supernatants or filtrates from solids-separation
76 processes are particularly promising nutrient sources, assuming that cyanobacterial strains can
77 efficiently use them.

78 Of the many streams available in common wastewater facilities, the liquid fraction of
79 anaerobic digestate is thought to be the most attractive nutrient source (8–11). Although digestate
80 is rich in the inorganic constituents necessary for growth, it also contains dissolved organic matter
81 (DOM) that has been shown to limit photosynthetic activity (12). DOM is a heterogenous mixture
82 of aliphatic and aromatic compounds derived from the decomposition of living organisms (13).
83 The chemical nature of wastewater-derived DOM is largely governed by the type of treated waste

84 and the treatment process, but it is largely comprised of hydrophilic, fulvic, and humic substances
85 (14, 15). Humics can induce damaging permeability in model and bacterial membranes (16, 17).
86 Various studies have also demonstrated that fulvic and humic acids can enhance the solubility of
87 many organic compounds (18), which in turn would augment their bioavailability and potential
88 membrane permeability. Many of these compounds are also photo-reactive, producing toxic
89 hydrogen peroxide and hydroxyl radicals (19, 20), which is of significant concern for phototroph
90 cultivation.

91 The mode of DOM toxicity is thought to involve interactions with the protein-pigment
92 complex of photosystem II (PSII) in photosynthetic organisms, although the exact molecular
93 mechanism remains unclear (21). When the rate of light induced damage to PSII exceeds its rate
94 of repair, growth suppression and chlorosis result from the phenomena known as photoinhibition
95 (22). When damage by photoinhibition is sufficient to hamper the natural ability to consume
96 electrons generated by photosynthesis, reactive oxygen species (ROS) are concomitantly produced
97 as an undesired by-product. Prolonged oxidative stress halts protein translation through oxidation
98 of specific cysteine residues in the ribosomal elongation factors (23). Given these findings, it is
99 increasingly evident that under conditions of sustained stress, regulation of electron flow is critical
100 to maintain homeostasis in photosynthetic organisms (24, 25). Thus, it is important to understand
101 the mechanisms by which DOM may be interrupting electron flow in order to capitalize on the
102 potential of cyanobacteria to remediate wastewater and generate high-value chemicals.

103 In this study, we tested the practicality of using combined streams from a municipal
104 wastewater plant as a nutrient source for cyanobacterial cultivation. We used the euryhaline
105 cyanobacterium *Synechococcus* sp. strain PCC 7002 (PCC 7002) due to its exceptional tolerance
106 to high light intensity, salt, and other environmental stresses (26, 27). Initial attempts to grow PCC

107 7002 in this nutrient source under standard environmental conditions for this strain (1% (v/v) CO_2,
108 a temperature of 37°C, and illumination of 200 μmol photons $m^{-2}s^{-1}$) resulted in photobleached
109 (white-yellow) cultures. In an effort to explain this observation while developing more feasible
110 cultivation conditions, we assessed the effects of many environmental parameters during PCC
111 7002 cultivation in wastewater-based media by monitoring changes in growth rate, photopigment
112 abundance, oxygen evolution rates, membrane integrity, and membrane composition. High GBF
113 concentrations were associated with elevated DOM levels. Decreased photosynthetic oxygen
114 production rates were also noted upon exposure to high levels of GBF. We observed marked
115 membrane permeability, photosystem degradation, low growth rates, and ROS production in
116 cultures exposed to GBF at 37°C. In comparison, at 27°C the cultures grown on GBF had reduced
117 membrane permeability, robust growth rates, as well as high levels of total fatty acids and an
118 elevated unsaturated fatty acid content relative to control. This suggests bioavailability of the
119 photoinhibitory compound in GBF is governed by changes in membrane content and composition
120 that occur during growth.
121

122 **MATERIALS AND METHODS**

123 *Media and Growth Conditions*

124 *Synechococcus* sp. strain PCC 7002 was obtained from the Pasteur Culture Collection of
125 Cyanobacteria. Experiments were performed with a strain of PCC 7002 harboring the *aaC1* gene
126 encoding a gentamicin resistance marker in the A2842 locus (*glpK*) to maintain axenic cultures.
127 Strains were grown and maintained on solid media composed of Medium A^+ (28) supplemented
128 with 5 μM $NiSO_4$ (29) with 1.5% Bacto-Agar. Strains were cultured from a single colony in 250

129 ml baffled flasks with 50 mL media with 1% CO_2-enriched air at 150 rpm in a Kuhner ISF1-X
130 orbital shaker. Temperature was maintained at 37°C or 27°C and light intensity was fixed at
131 approximately 200 µmol photons $m^{-2}s^{-1}$ or 100 µmol photons $m^{-2}s^{-1}$ via a custom LED panel.
132 Strains were pre-acclimated to the culture conditions overnight before inoculating in fresh media.
133 Optical density at 730 nm was measured in a Tecan M1000 plate reader.

134 Wastewater-derived media was obtained from the Nine Springs Wastewater Treatment
135 Plant (Dane County, Wisconsin, USA). The plant is configured for biological nutrient removal via
136 a modified University of Cape Town process with no internal nitrate recycling and stable
137 performance yielding high secondary effluent quality (total phosphorus < 1 mg P/L, ammonia < 1
138 mg N/L, nitrate ~ 15 mg N/L) (30). Anaerobic digesters are used for solids stabilization and the
139 resulting digested material is passed over a gravity belt filter for dewatering. The system includes
140 an Ostara WASSTRIP process to recover phosphorus. This filtrate (GBF) served as the primary
141 source of phosphorus and reduced nitrogen for our cultures, and effluent from the post-mainstream
142 secondary treatment clarifier (secondary effluent) served as a diluent. GBF was gravity filtered
143 through a paper coffee filter to remove any exceptionally large flocs, then stored at -80°C until
144 use. Secondary effluent was collected one to four days before each experiment and held under
145 refrigeration at approximately 2°C. Experimental media was comprised primarily of secondary
146 clarifier effluent and GBF, combined in different proportions. Unless otherwise noted, GBF was
147 used at a concentration of 12.5% (v/v) in secondary effluent, supplemented with trace metals and
148 vitamin B12 at the concentrations found in Medium A^+, as well as KH_2PO_4 at a molar ratio of 1:32
149 soluble reactive phosphorus (SRP) to bioavailable nitrogen (the sum of NH_4^+ and NO_3^-). All media
150 was buffered with Tris-HCl and adjusted to pH 8.0 with potassium hydroxide or hydrochloric acid

151 before sterilization by autoclaving, and gentamycin was added at working concentrations (30
152 μg/mL) after cooling.

153 *Staining, Flow Cytometry, and Fluorescence Measurements*

154 The membrane permeability of cyanobacteria cells was recorded by a flow cytometer
155 (FACSCalibur, BD Biosciences, San Jose, CA, USA). After growth in the respective media, cells
156 were centrifuged (2 minutes, 5000 RCF), decanted, and resuspended in 1 mL of Tris-Buffered
157 Saline (TBS) solution (pH 8.0). To identify membrane-compromised cells, SYTOX Green (Life
158 Technologies) was also added to each sample (1 μM). SYTO 59 (Life Technologies) was added to
159 each sample (1 μM) as a nucleic acid counterstain. As a control for a permeabilized membrane,
160 cells were resuspended in 190 proof ethanol. SYTOX green fluorescence was visualized using 488
161 nm laser excitation and emission area was read using a 530/30 nm bandpass filter. The 633 nm
162 laser coupled with a 661/16 bandpass filter was used for SYTO 59 visualization. Analysis of the
163 cytometric data was carried out with CellQuest Pro (BDBiosciences, San Jose,CA, USA) software.

164 To assess reactive oxygen species production, cells (OD_{730} = 1) were incubated overnight
165 in Medium A^+, 12.5 % (v/v) GBF, 12.5 % (v/v) GBF + 1 mM Dithiothreitol (DTT), 12.5 % (v/v)
166 GBF + 1 mM N-acetylcysteine (NAC), or Medium A^+ + 100 μM methyl viologen as a positive
167 control at 37°C with 5% CO_2 at a light intensity of 200 μmol photons $m^{-2}s^{-1}$. Cells were washed in
168 TBS, and either Sytox Green (1 μM) or CellROX Orange reagent (Life Technologies) (5 μM) was
169 added. After 30 min incubation in darkness at 37°C, fluorescence was measured (Ex/Em 545/565
170 nm for Cell ROX Orange) and (Ex/Em 504/523 nm for Sytox Green) in a Tecan M1000 plate
171 reader.

172 *GBF Characterization*

173 SRP, ammonia, nitrate, and nitrite concentrations were determined for all secondary
174 clarifier effluent and GBF samples used in these experiments. In addition, the GBF was tested for
175 total suspended solids (TSS), volatile suspended solids (VSS) total solids (TS), and chemical
176 oxygen demand (COD). Ammonia, SRP, and COD concentrations were determined by
177 colorimetric tests using reagents from Hach. Nitrate and nitrite were determined using high
178 performance liquid chromatography (Shimadzu) with a C18 column and photodiode array detector
179 (31). TSS, VSS, and TS were measured according to Standard Method 2540 D, 2540 E, and 2540
180 B, respectively, with 47mm diameter glass fiber filters (Whatman) used for TSS and VSS (32).
181 Fluorescence EEM measurements and UV-Vis absorbance scans were conducted using a M1000
182 Tecan plate reader using a UV-transparent plate (Costar 3635). Fluorescence intensity was
183 normalized to quinine sulfate units (QSU), where 1 QSU is the maximum fluorescence intensity
184 of 1 ppm of quinine sulfate in 0.1 N H_2SO_4 at Ex/Em = 350/450. Rayleigh scatter effects were
185 removed from the data set.

186 *Biochemical analyses*

187 Batch cultures were further assayed for dry cell weight (DCW), fatty acid content, oxygen
188 evolution rates, and chlorophyll a content. Cells were concentrated by centrifugation, washed in
189 TBS, and lyophilized overnight to obtain dry cell weights (DCW). Fatty acids from approximately
190 10 mg of DCW with 10 mg ml^{-1} pentadecanoic acid as an internal standard were converted to
191 methyl-esters, extracted with n-hexane and analyzed by GC-FID on a Restek Stabilwax column
192 (60m, 0.53 mm ID, 0.50 μm) (33). Photosynthetic oxygen evolution from whole cells was
193 measured with a Unisense MicroOptode oxygen electrode with 10 mM $NaHCO_3$ illuminated with
194 a slide projector at photosynthetic photon flux densities ranging from 76-2700 μmol
195 photons photons m^{-2} s^{-1} for 30 min at room temperature (34). Cells were collected by

196 centrifugation and resuspended in the appropriate media to give an OD_{730} = 1.0. Chlorophyll a
197 measurements were done via a 100% chilled methanol extraction procedure (35). Chlorophyll a
198 was calculated via the following equation: $Chl_a = 16.29 * A^{665} - 8.54 * A^{652}$ (36).

199 **RESULTS**

200 *GBF and secondary effluent characteristics*

201 We measured nutrient concentrations from the batches of GBF collected over the 6 month
202 experimental period (Table 1 and Table 2), to ascertain if it was a stable and reliable nutrient source
203 for cultivating the cyanobacteria. Sampling points from the Nine Springs Wastewater Treatment
204 Plant (Dane County, Wisconsin, USA) are shown in Figure 1. In order to calculate nutrient
205 stoichiometries, we took the sum of NH_3-N and NO_3-N to be the bioavailable N. Nutrient levels
206 in the GBF were markedly more variable than in the secondary effluent. The average molar ratio
207 of bioavailable N to SRP was 35 ± 7 in GBF (12.5% v/v) diluted with secondary effluent, as
208 compared to 32 in Medium A^+.

209 We also measured DOM quality in the secondary effluent and GBF using
210 excitation−emission matrix (EEM) fluorescence spectroscopy (37) because we hypothesized that
211 DOM was linked to toxicity during cultivation, as has been shown in prior studies (16, 17, 38).
212 EEM fluorescence spectroscopy revealed that secondary effluent contained diffuse constituents,
213 including humic [excitation wavelengths (>280 nm) and emission wavelengths (>380 nm)] and
214 fulvic acid-like [excitation wavelengths (<250 nm) and emission wavelengths (>350 nm)] spectra
215 relative to Medium A^+ (Figure 2). The distinction between the two substances is historically based
216 on solubility (39), but compositionally, fulvic acids contain more acidic functional groups than
217 humic acids (40). The fulvic acid content in media preparations rose with increasing GBF
218 concentrations. Additionally, at high concentrations of GBF, we detected absorbance in a distinct

219 region [excitation wavelengths (270 -290 nm) and emission wavelengths (340-400 nm)] that points
220 to the presence of soluble microbial products, which include aromatic amino acids, carbohydrates,
221 or phenols (37, 41). Prior work has shown that the GBF stream of the Nine Springs Treatment
222 Plant contained high molecular weight DOM, which was dissimilar in composition to other
223 internal streams (42)

224 *Dose-dependent tolerance to GBF is a function of growth temperature*

225 To evaluate the effects of GBF dosage on PCC 7002 physiology, we measured biomass
226 accumulation (Figure 3) and growth rates (Table 3) in media with GBF concentrations ranging
227 from 6.25%-12.5% (v/v), as a function of temperature (27°C vs 37°C) and light intensity (100
228 μmol photons m^{-2} s^{-1} vs 200 μmol photons m^{-2} s^{-1}). Medium A^+ served as a control. Higher
229 temperatures depressed growth rates in GBF-based media. At 37°C, growth rates with 6.25% GBF
230 at both 100 μmol photons m^{-2} s^{-1} and 200 μmol photons m^{-2} s^{-1} were most comparable to Medium
231 A^+. Higher GBF concentrations had a more extreme effect on growth rates. However, this dose-
232 dependent effect of GBF on growth rate was abolished when the cultivation temperature was
233 lowered to 27°C. At 200 μmol photons m^{-2} s^{-1} and 27°C, GBF cultures grew twice as slowly as
234 the control and there was no significant difference between the tested GBF concentrations. Under
235 100 μmol photons m^{-2} s^{-1} and 27°C, growth rates were comparable across media conditions. Thus,
236 successful cultivation using the more concentrated GBF media required adjusting both the light
237 and temperature regimes.

238 *Dose-dependent membrane permeability of GBF is a function of growth temperature*

239 We wondered whether the decreased growth rates in GBF at 37°C was a result of
240 membrane permeability, given the known effect of humic acids on membrane integrity (16, 17).

241 To track the dynamics of GBF induced membrane permeability, we employed forward scatter flow
242 cytometry using SYTO 59 as a counterstain to identify cells, which were subsequently visualized
243 for membrane permeability using Sytox Green. As Sytox Green is a membrane impermeable dye
244 that fluoresces when binding to nucleic acids (43), fluorescence would indicate compromised outer
245 membrane structures. Two distinct phases were identified upon exposure to GBF, which we
246 interpreted as initial and chronic membrane permeability (Figure 4). Initial membrane permeability
247 was defined as the Sytox Green positive events for samples analyzed within the first 10 hours of
248 growth, while chronic membrane permeability accounted for the Sytox Green positive events
249 during subsequent time points. As was the case for growth rate, a relationship between both initial
250 and chronic membrane permeability and increasing GBF concentrations was found at 37°C (Figure
251 4a). While we still detected considerable initial membrane permeability with GBF exposure at
252 27°C, chronic membrane permeability decreased over time, mostly likely to the increase in
253 biomass (Figure 3). Altogether, this suggested that there was a temperature dependent adaptation
254 that ameliorated the susceptibility of cultures to GBF induced membrane permeability.

255 *Exposure to GBF at high temperatures generates radicals and destroys the photosynthetic*
256 *pigments*

257 We directly measured the ROS content and membrane permeability in response to
258 overnight GBF exposure at 37°C using the fluorophores Sytox Green and CellROX Orange (Figure
259 5). We examined the capacity of reducing agents Dithiothreitol (DTT) or N-acetylcysteine (NAC)
260 to quench the media toxicity, since they have anti-oxidant properties due to the direct reduction of
261 disulfide bonds or as precursors for the anti-oxidant glutathione (44). To measure their effect on
262 the ROS production and culture viability after GBF exposure, we assessed ROS content and
263 membrane integrity with either concurrent addition or preincubation of these quenching

264 compounds in the diluted (12.5% v/v) GBF media. Addition of 100 μM methyl viologen to
265 Medium A^+ served as a positive control. Exposure of cells to 12.5%-GBF media resulted in marked
266 ROS production and membrane permeability, which no thiol treatment alleviated.

267 Photobleaching of the photosynthetic pigments is also a common symptom of oxidative
268 stress in photosynthetic organisms and is caused by the accumulation of ROS (45). To investigate
269 the effects of GBF media on the photosynthetic pigmentation, we performed whole cell absorbance
270 scans of cultures cultivated at two different temperatures (27°C vs 37°C) and the same light
271 intensity (200 μmol photons m^{-2} s^{-1}). High GBF concentrations yielded enhanced chlorophyll,
272 phycobilisome, and carotenoid degradation at 37°C (Figure 7a). At 27°C, photosynthetic pigments
273 maintained intact relative to the control, regardless of GBF concentration, implying less ROS
274 production at this temperature (Figure 7b).

275 *Exposure to GBF retards oxygen evolution*

276 To better delineate the cause of initial toxicity associated with high GBF concentrations,
277 we measured maximal oxygen evolution rates for strains briefly exposed to media with 12.5% v/v
278 GBF while increasing the light intensity. Measurements of photosynthetic oxygen evolution would
279 allow for an indirect assessment of PSII activity and electron transfer (46). Cultures were grown
280 to early linear phase in Medium A^+ or GBF media, washed, and resuspended in the appropriate
281 media. Resuspension media was saturated with HCO_3^- (10 mM) in order to prevent inorganic
282 carbon limitation. As expected, cells grown and assayed in Medium A^+ at 37°C showed a clear
283 increase in O_2 evolution rate as the light intensity approached saturation at 2700 μm photons
284 m^{-2} s^{-1}, reaching a maximal rate of 240 ± 8 μmol O_2 (mg Chl a)$^{-1}$ h^{-1} (Figure 7a). Cells grown in
285 Medium A^+ at 37°C but assayed in 12.5% GBF had diminished O_2 evolution rates at all light
286 intensities, plateauing with a rate of 79 ± 6 μmol O_2 (mg Chl a)$^{-1}$ h^{-1} at an intensity of 270 μmol

287 photons m^{-2} s^{-1} (Figure 7a). Thus, exposure to GBF under these conditions caused an immediate
288 decrease in O_2 production.

289 Next, we examined the effect of temperature in a similar experiment. Assays carried out in
290 Medium A^+ after growth in Medium A^+ at 27°C showed much higher maximal O_2 evolution rates
291 at all tested light intensities than with cells grown at 37°C (Figure 7b), peaking at a rate 556 ± 102
292 μmol O_2 (mg Chl a)$^{-1}$ h^{-1}). This was expected because elevated O_2 evolution rates in low
293 temperature grown cells have been previously reported and were attributed to a substantial change
294 in photosystem stoichiometry (47). The O_2 evolution rates of cells grown in Medium A^+ at 27°C
295 and then resuspended in 12.5% GBF stayed relatively constant at all of the tested intensities and
296 were roughly 5-fold lower than in controls, with a maximal rate of 109 ± 22 μmol O_2 (mg Chl a)$^{-}$
297 ^{1} h^{-1} at an intensity of 75 μmol photons m^{-2} s^{-1}. We compared the above rates to those from
298 cultures grown in 12.5% GBF at 27°C to test if adaptation to GBF was met with changes in
299 photosynthetic activity. At the examined light intensities, O_2 evolution rates with 27°C GBF-
300 adapted cultures were not statistically different from those measured in cultures grown at the same
301 temperature in Medium A^+. Finally, we conducted the inverse experiment, using cultures grown
302 in GBF media at 27°C but assayed in Medium A^+ under saturating light. Interestingly, they
303 displayed the highest evolution rate of any tested condition, at 944 ± 96 μmol O_2 (mg Chl a)$^{-1}$ h^{-1}
304 (Figure 7b). This suggested that there is a period of dynamic photosynthetic adaptation to
305 overcome the stress of GBF, and that when the stress is removed, the cells have an enhanced
306 capacity for photosynthetic activity.

307 Additional assays were performed at light saturation (2700 μmol m^{-2} s^{-1}) with cultures
308 adapted to 37°C (Figure 8) to further examine the effects of media conditions on oxygen evolution
309 rates. Again, oxygen evolution rates in GBF (73 ± 8 μmol O_2 (mg Chl a)$^{-1}$ h^{-1}) were much lower

310 than Medium A^+ (248 ± 21 μmol O_2 (mg Chl a)$^{-1}$ h^{-1}). In order to rule out the effect of differences
311 in overall ionic strength, we increased the osmolarity of the GBF medium by adding NaCl to match
312 the levels found in Medium A^+, and found no statistical difference in oxygen evolution as
313 compared to experiments without added NaCl. Attempts to eliminate the inhibitory effect of GBF
314 on oxygen evolution by gravity filtration through powdered activated carbon were unsuccessful.
315 We also measured oxygen evolution rates in control experiments designed to inhibit
316 photosynthetic electron transfer through 10 μM DCMU addition to Medium A^+ (48), and to prevent
317 de-novo protein synthesis by pre-treating cultures with 800 μg ml^{-1} Lincomycin in Medium A^+
318 (49), prior to incubation at light saturation for 1 hour. However, evolution rates with these controls
319 were higher than those treated with GBF. Therefore, no definitive conclusion about the molecular
320 mechanism responsible for reduced oxygen evolution rates in the presence of GBF could be made.

321 *Acclimation to GBF changes lipid content and composition*

322 Based on the results described above, we hypothesized that the temperature dependent
323 adaptation may be related to changes in membrane content and composition. We extracted total
324 fatty acids of cultures grown at 27°C for 72 hours in 12.5% GBF or Medium A^+, and analyzed the
325 content after derivatization. We could detect and resolve all major saturated and unsaturated fatty
326 acid species (Table 4). Cultures grown in GBF had greater totals of assayed fatty acid species (27
327 ± 7 mg FAME gDCW^{-1}) when compared to cells grown in Medium A^+ (15 ± 1 mg FAME gDCW^{-}
328 ^{1}) (Table 4). The most abundant fatty acid in all samples was 16:0 (42-45% of the total fatty acids).
329 C18:2 Δ9,12 fatty acids comprised a significant fraction of Medium A^+ grown cultures with 22%
330 of the total fatty acid species. However, in GBF-grown cells C18:2 Δ9,12 fatty acids were only
331 15% of the total fatty acid pool, while C18:3 Δ9,12,15 fatty acids were twice as high in GBF grown
332 cells (16%) than in Medium A^+ grown cells (9%) (Table 4). These results suggest that cells were

333 altering their membrane homeostasis when grown in GBF, as compared to standard growth in
334 Medium A^+. While we did not differentiate the fatty acid content and composition between the
335 outer, plasma, or thylakoid membranes in our study, prior work done with the cyanobacterium
336 *Synechocystis* PCC 6803 found similar fatty acid composition between thylakoid and plasma
337 membranes (50).

338 **DISCUSSION**

339 The amount and distribution of arable land and potable water are projected to change over
340 the next several decades due to climate change, while the rise in global population and standard of
341 living are expected to increase demand for these resources (51). Microalgal cultivation integrated
342 with industrial and municipal wastewater treatment circumvents many of the resource concerns
343 raised over biofuel production (2), while simultaneously removing additional nutrients and
344 pollutants present in the wastewater (52). *Synechococcus* PCC 7002 is an intriguing possible
345 platform for this purpose, since it can be readily engineered to produce high-value chemicals (53).
346 However, under standard environmental conditions we were unable to obtain robust growth of
347 PCC 7002 using a diluted municipal side stream (GBF) as a nutrient source. We hypothesized that
348 this effect may be due to the presence of DOM, which has been demonstrated to cause a decrease
349 in photosynthetic performance in various cyanobacteria strains (54–56). We investigated the
350 effects of light intensity and temperature on the physiology of cultures grown in GBF, in an effort
351 to find conditions conducive to high growth rates and biomass generation, and to better understand
352 the mechanisms of GBF toxicity.

353 We propose that the herbicidal effect of GBF is primarily due to PSII inhibition as shown
354 in Figures 7 and 8, brought about by quinone or phenolic compounds within the "soluble microbial
355 products" found in our EEM scans (Figure 2). Humic material enriched in quinone and phenolic

356 compounds can inhibit cyanobacterial growth (57, 58). Phenolic photosynthetic electron transfer
357 inhibitors, such as 2,5-Dibromo-3-methyl-6-isopropyl-p-benzoquinone (DBMIB), alter the redox
358 potential of the PQ pool of PSII by blocking forward electron transfer to the cytochrome b_6/f
359 complex (59). The immediate decrease in oxygen evolution (Figure 7) and high rates of initial
360 membrane permeability (Figure 4) upon GBF exposure suggests that the toxic compound(s)
361 rapidly cross the outer membrane, where it subsequently interrupts photosynthetic electron flow.
362 Chronic exposure to phenolic herbicides eventually leads to radical-catalyzed back reactions that
363 trigger ROS formation (60) (Figure 5) that facilitates complex destruction (Figure 6) and cell death
364 (45, 61–64). Some phenolic herbicides may also act as arylating agents, causing covalent binding
365 to macromolecules via Michael addition and thiol pool depletion (65). The inability of the reducing
366 agents we tested to maintain membrane integrity suggests that GBF-induced cytomembrane
367 permeability is likely caused by redox cycling, and not arylation.

368 We found that cultivation temperature was an important factor determined whether PCC
369 7002 could grow under high GBF concentrations. Numerous physiological processes are altered
370 at low temperatures (66). Notably, the fatty acyl chains in membranes undergo a transition from a
371 fluid to nonfluid state (67). Cyanobacterial membrane organization is complicated by the
372 simultaneous existence of the outer, plasma, and thylakoid membranes, each with a designated
373 physiological function (68). As part of the homeoviscous response upon a shift to a lower
374 temperature, cyanobacteria alter the expression of desaturases in their plasma and thylakoid
375 membranes (69) to increase unsaturated fatty acid content and maintain optimal membrane
376 function (70). Optimal thylakoid membrane fluidity is a critical factor in photosynthetic electron
377 transport, because co-utilized redox components must be able to move quickly between
378 photosynthetic and respiratory complexes to ensure ideal electron flow (71, 72). Temperature is

379 known to influence the kinetics governing the redox state of plastiquinone (PQ) through alterations
380 in thylakoid membrane composition and fluidity (73). We hypothesize that alteration of the
381 thylakoid membrane to circumvent GBF induced changes in the overall redox state is also an
382 important component of the adaptive response to lower temperatures, given the increase in total
383 unsaturated fatty acids observed during cultivation in GBF-based media (Table 4). Upon shifts to
384 a lower temperature (74), PCC 7002 has also been shown to translocate the phycobilisomes from
385 PSII to PSI, thereby decreasing the ratio of reducing power to proton-motive force (75). Mutant
386 cells of the cyanobacterium *Synechocystis* PCC 6803 that lacked polyunsaturated fatty acids were
387 unable to perform these state transitions at low temperatures (76). This change in photosystem
388 arrangement at 27°C may also contribute to acclimation to the photoinhibitory compound. Future
389 efforts to increase tolerance to these toxicants might include disruption of the inhibitor binding
390 sites (77, 78) or optimizing thylakoid membrane fluidity (79).

391 **CONCLUSIONS**

392 Under standard cultivation conditions of 37°C with the cyanobacteria *Synechococcus* sp.
393 strain PCC 7002, there was a dose-dependent relationship between liquid anaerobic digestate
394 (GBF) concentration and membrane permeability. This dose-dependent relationship mirrored ROS
395 production and photopigment degradation. Digestate contained dissolved organic matter
396 constituents that were likely affecting photosynthetic electron transport. Decreasing the cultivation
397 temperature to 27°C enabled robust cultivation at high digestate concentrations, resulting in high
398 biomass productivities. This temperature dependent tolerance may be due to changes in membrane
399 properties. Our study highlights an unanticipated influence of dissolved organic matter on
400 photosynthetic growth and physiology in wastewater based media, as well as a potential
401 mechanism for tolerance in low temperatures.

ACKNOWLEDGEMENTS

This work was funded by the US National Science Foundation (EFRI-1240268). TCK is the recipient of a National Institutes of Health (NIH) Biotechnology Training Fellowship (NIGMS-5 T32 GM08349) and a fellowship from the UW-Madison College of Engineering's Graduate Engineering Research Scholars (GERS) program. The authors are grateful to Richard Mikel, Matthew Dysthe, and Derek Jacobs for help with routine sampling, and Andrew Maizel and Christina Remucal for advice on the excitation−emission matrix (EEM) fluorescence spectroscopy.

REFERENCES

1. Oliver JWK, Atsumi S. 2014. Metabolic design for cyanobacterial chemical synthesis. Photosynth Res 120:249–61.
2. Pate R, Klise G, Wu B. 2011. Resource demand implications for US algae biofuels production scale-up. Appl Energy 88:3377–3388.
3. Clarens AF, Resurreccion EP, White M a, Colosi LM. 2010. Environmental life cycle comparison of algae to other bioenergy feedstocks. Environ Sci Technol 44:1813–9.
4. Posadas E, García-Encina PA, Domínguez A, Díaz I, Becares E, Blanco S, Muñoz R. 2014. Enclosed tubular and open algal-bacterial biofilm photobioreactors for carbon and nutrient removal from domestic wastewater. Ecol Eng 67:156–164.
5. Sturm BSM, Lamer SL. 2011. An energy evaluation of coupling nutrient removal from wastewater with algal biomass production. Appl Energy 88:3499–3506.
6. Hoffmann JP. 1998. Wastewater Treatment with Suspended and Nonsuspended Algae. J Phycol 34:757–763.
7. de la Noüe J, Laliberté G, Proulx D. 1992. Algae and waste water. J Appl Phycol 4:247–254.
8. Olguín EJ. 2012. Dual purpose microalgae–bacteria-based systems that treat wastewater and produce biodiesel and chemical products within a Biorefinery. Biotechnol Adv 30:1031–1046.
9. Wang L, Min M, Li Y, Chen P, Chen Y, Liu Y, Wang Y, Ruan R. 2010. Cultivation of green algae Chlorella sp. in different wastewaters from municipal wastewater treatment plant. Appl Biochem Biotechnol 162:1174–86.
10. Peccia J, Haznedaroglu B, Gutierrez J, Zimmerman JB. 2013. Nitrogen supply is an

important driver of sustainable microalgae biofuel production. Trends Biotechnol 31:134–8.

11. Rawat I, Ranjith Kumar R, Mutanda T, Bux F. 2011. Dual role of microalgae: Phycoremediation of domestic wastewater and biomass production for sustainable biofuels production. Appl Energy 88:3411–3424.

12. Pflugmacher S, Spangenberg M, Steinberg CEW. 1999. Dissolved organic matter (DOM) and effects on the aquatic macrophyte Ceratophyllum demersum in relation to photosynthesis, pigmentpattern and activity of detoxication enzymes. J Appl Bot 73:184–190.

13. Zsolnay Á. 2003. Dissolved organic matter: Artefacts, definitions, and functions, p. 187–209. *In* Geoderma.

14. Imai A, Fukushima T, Matsushige K, Kim Y-H, Choi K. 2002. Characterization of dissolved organic matter in effluents from wastewater treatment plants. Water Res 36:859–870.

15. Akhiar A, Torrijos M, Battimelli A, Carrère H. 2016. Comprehensive characterization of the liquid fraction of digestates from full-scale anaerobic co-digestion. Waste Manag.

16. Vigneault B, Percot A, Lafleur M, Campbell PGC. 2000. Permeability changes in model and phytoplankton membranes in the presence of aquatic humic substances. Environ Sci Technol 34:3907–3913.

17. Ojwang' LM, Cook RL. 2013. Environmental Conditions That Influence the Ability of Humic Acids to Induce Permeability in Model Biomembranes. Environ Sci Technol 47:8280–8287.

18. Chiou CT, Malcolm RL, Brinton TI, Kile DE. 1986. Water solubility enhancement of some organic pollutants and pesticides by dissolved humic and fulvic acids. Environ Sci

Technol;(United States) 20.

19. Zhang D, Yan S, Song W. 2014. Photochemically Induced Formation of Reactive Oxygen Species (ROS) from Effluents Organic Matter. Environ Sci Technol.

20. Lee E, Glover CM, Rosario-Ortiz FL. 2013. Photochemical formation of hydroxyl radical from effluent organic matter: Role of composition. Environ Sci Technol 47:12073–12080.

21. Laue P, Bährs H, Chakrabarti S, Steinberg CEW. 2014. Natural xenobiotics to prevent cyanobacterial and algal growth in freshwater: Contrasting efficacy of tannic acid, gallic acid, and gramine. Chemosphere 104:212–220.

22. Keren N, Krieger-Liszkay A. 2011. Photoinhibition: molecular mechanisms and physiological significance. Physiol Plant 142:1–5.

23. Nagano T, Kojima K, Hisabori T, Hayashi H, Morita EH, Kanamori T, Miyagi T, Ueda T, Nishiyama Y. 2012. Elongation factor G is a critical target during oxidative damage to the translation system of Escherichia coli. J Biol Chem 287:28697–704.

24. Foyer CH, Neukermans J, Queval G, Noctor G, Harbinson J. 2012. Photosynthetic control of electron transport and the regulation of gene expression. J Exp Bot 63:1637–61.

25. Voss I, Sunil B, Scheibe R, Raghavendra AS. 2013. Emerging concept for the role of photorespiration as an important part of abiotic stress response. Plant Biol (Stuttg) 15:713–22.

26. Ruffing AM. 2011. Engineered cyanobacteria: Teaching an old bug new tricks. bioe 2:136–149.

27. Xu Y, Alvey RM, Byrne PO, Graham JE, Shen G, Bryant DA. 2011. Expression of genes in cyanobacteria: adaptation of endogenous plasmids as platforms for high-level gene expression in Synechococcus sp. PCC 7002. Methods Mol Biol 684:273–93.

28. Stevens SE, Patterson COP, Myers J. 1973. The Production of Hydrogen Peroxide by Blue-Green Algae: A Survey. J Phycol 9:427–430.

29. Sakamoto T, Bryant DA. 2001. Requirement of Nickel as an Essential Micronutrient for the Utilization of Urea in the Marine Cyanobacterium Synechococcus sp. PCC 7002. Microbes Environ 16:177–184.

30. Flowers JJ, Cadkin TA, McMahon KD. 2013. Seasonal bacterial community dynamics in a full-scale enhanced biological phosphorus removal plant. Water Res 47:7019–7031.

31. He S, McMahon KD. 2011. "Candidatus Accumulibacter" gene expression in response to dynamic EBPR conditions. ISME J 5:329–40.

32. Eaton AD, Franson MAH. 2005. Standard Methods for the Examination of Water & Wastewater, 21sted. American Public Health Association.

33. Lennen RM, Braden DJ, West RA, Dumesic JA, Pfleger BF. 2010. A process for microbial hydrocarbon synthesis: Overproduction of fatty acids in Escherichia coli and catalytic conversion to alkanes. Biotechnol Bioeng 106:193–202.

34. Sakamoto T, Bryant D a. 2002. Synergistic effect of high-light and low temperature on cell growth of the Delta12 fatty acid desaturase mutant in Synechococcus sp. PCC 7002. Photosynth Res 72:231–42.

35. Miyashita H, Adachi K, Kurano N, Ikemot H, Chihara M, Miyach S. 1997. Pigment composition of a novel oxygenic photosynthetic prokaryote containing chlorophyll d as the major chlorophyll. Plant cell Physiol 38:274–281.

36. Porra RJ, Thompson WA, Kriedemann PE. 1989. Determination of accurate extinction coefficients and simultaneous equations for assaying chlorophylls a and b extracted with four different solvents: verification of the concentration of chlorophyll standards by atomic

absorption spectroscopy. Biochim Biophys Acta (BBA)-Bioenergetics 975:384–394.

37. Chen W, Westerhoff P, Leenheer JA, Booksh K. 2003. Fluorescence Excitation-Emission Matrix Regional Integration to Quantify Spectra for Dissolved Organic Matter. Environ Sci Technol 37:5701–5710.

38. Neilen A, W. Hawker D, R. O'Brien K, Burford M. 2017. Phytotoxic effects of terrestrial dissolved organic matter on a freshwater cyanobacteria and green algae species is affected by plant source and DOM chemical compositionChemosphere.

39. Lehmann J, Kleber M. 2015. The contentious nature of soil organic matter. Nature 1–9.

40. Peña-méndez ME, Havel J, Patočka J. 2005. Humic substances – compounds of still unknown structure : applications in agriculture , industry , environment , and biomedicine. J Appl Biomed 3:13–24.

41. Cowgill RW. 1963. Fluorescence and the structure of proteins. I. Effects of substituents on the fluorescence of indole and phenol compounds. Arch Biochem Biophys 100:36–44.

42. Maizel AC, Remucal CK. 2017. The effect of advanced secondary municipal wastewater treatment on the molecular composition of dissolved organic matter. Water Res 122:42–52.

43. Roth BL, Poot M, Yue ST, Millard PJ. 1997. Bacterial viability and antibiotic susceptibility testing with SYTOX green nucleic acid stain. Appl Environ Microbiol 63:2421–31.

44. Samuni Y, Goldstein S, Dean OM, Berk M. 2013. The chemistry and biological activities of N-acetylcysteine. Biochem Biophys 1830:4117–4129.

45. Latifi A, Ruiz M, Zhang C-C. 2009. Oxidative stress in cyanobacteria. FEMS Microbiol Rev 33:258–78.

46. van Gorkom HJ, Gast P. 1996. Measurement of Photosynthetic Oxygen Evolution, p. 391–405. *In* Amesz, J, Hoff, AJ (eds.), Biophysical Techniques in Photosynthesis. Springer

Netherlands, Dordrecht.

47. Sakamoto T, Bryant D a. 1998. Growth at low temperature causes nitrogen limitation in the cyanobacterium Synechococcus sp. PCC 7002. Arch Microbiol 169:10–9.

48. Huber SC, Edwards GE. 1975. Effect of DBMIB, DCMU and antimycin A on cyclic and noncyclic electron flow in C4 mesophyll chloroplasts. FEBS Lett 58:211–214.

49. Tyystjärvi E, Aro EM. 1996. The rate constant of photoinhibition, measured in lincomycin-treated leaves, is directly proportional to light intensity. Proc Natl Acad Sci U S A 93:2213–2218.

50. Los DA, Murata N. 1996. Characterization of the Fad12 mutant of Synechocystis that is defective in Δ12 acyl-lipid desaturase activity. Biochim Biophys Acta - Lipids Lipid Metab 1299:117–123.

51. Parry ML, Rosenzweig C, Iglesias A, Livermore M, Fischer G. 2004. Effects of climate change on global food production under SRES emissions and socio-economic scenarios. Glob Environ Chang 14:53–67.

52. Wang Y, Ho SH, Cheng CL, Guo WQ, Nagarajan D, Ren NQ, Lee DJ, Chang JS. 2016. Perspectives on the feasibility of using microalgae for industrial wastewater treatment. Bioresour Technol 222:485–497.

53. Davies FK, Work VH, Beliaev AS, Posewitz MC. 2014. Engineering Limonene and Bisabolene Production in Wild Type and a Glycogen-Deficient Mutant of Synechococcus sp. PCC 7002. Front Bioeng Biotechnol 2:1–11.

54. Sun B, Tanji Y, Unno H. 2006. Extinction of cells of cyanobacterium Anabaena circinalis in the presence of humic acid under illumination. Appl Microbiol Biotechnol 72:823–828.

55. Shao J, Wu Z, Yu G, Peng X, Li R. 2009. Allelopathic mechanism of pyrogallol to

Microcystis aeruginosa PCC7806 (Cyanobacteria): From views of gene expression and antioxidant system. Chemosphere 75:924–928.

56. Gjessing ET, Alberts J., Bruchet A, Egeberg PK, Lydersen E, McGown LB, Mobed JJ, Münster U, Pempkowiak J, Perdue M, Ratnawerra H, Rybacki D, Takacs M, Abbt-Braun G. 1998. Multi-method characterisation of natural organic matter isolated from water: characterisation of reverse osmosis-isolates from water of two semi-identical dystrophic lakes basins in Norway. Water Res 32:3108–3124.

57. Bährs H, Putschew A, Steinberg CEW. 2013. Toxicity of hydroquinone to different freshwater phototrophs is influenced by time of exposure and pH. Environ Sci Pollut Res 20:146–154.

58. Bährs H, Menzel R, Kubsch G, Stößer R, Putschew A, Heinze T, Steinberg CEW. 2012. Does quinone or phenol enrichment of humic substances alter the primary compound from a non-algicidal to an algicidal preparation? Chemosphere 87:1193–1200.

59. Schoepp B, Brugna M, Riedel A, Nitschke W, Kramer DM. 1999. The Qo-site inhibitor DBMIB favours the proximal position of the chloroplast Rieske protein and induces a pK-shift of the redox-linked proton. FEBS Lett 450:245–250.

60. Pallett KE, Dodge AD. 1980. Studies into the Action of Some Photosynthetic Inhibitor Herbicides. J Exp Bot 31:1051–1066.

61. Krieger-Liszkay A, Fufezan C, Trebst A. 2008. Singlet oxygen production in photosystem II and related protection mechanism. Photosynth Res 98:551–564.

62. Idedan I, Tomo T, Noguchi T. 2011. Herbicide effect on the photodamage process of photosystem II: Fourier transform infrared study. Biochim Biophys Acta - Bioenerg 1807:1214–1220.

63. Nishiyama Y, Allakhverdiev SI, Murata N. 2011. Protein synthesis is the primary target of reactive oxygen species in the photoinhibition of photosystem II. Physiol Plant 142:35–46.

64. Dominy PJ, Williams WP. 1987. Chlorophyll Photobleaching is Dependent on Photosystem II Inhibition, p. 35–38. *In* Biggins, J (ed.), Progress in Photosynthesis Research: Volume 4 Proceedings of the VIIth International Congress on Photosynthesis Providence, Rhode Island, USA, August 10--15, 1986. Springer Netherlands, Dordrecht.

65. Wang X, Thomas B, Sachdeva R, Arterburn L, Frye L, Hatcher PG, Cornwell DG, Ma J. 2006. Mechanism of arylating quinone toxicity involving Michael adduct formation and induction of endoplasmic reticulum stress. Proc Natl Acad Sci U S A 103:3604–9.

66. Morgan-Kiss RM, Priscu JC, Pocock T, Gudynaite-Savitch L, Huner NPA. 2006. Adaptation and Acclimation of Photosynthetic Microorganisms to Permanently Cold Environments. Microbiol Mol Biol Rev 70:222–252.

67. De Mendoza D. 2014. Temperature Sensing by Membranes. Annu Rev Microbiol 68:101–16.

68. Pisareva T, Kwon J, Oh J, Kim S, Ge C, Wieslander A, Choi J-S, Norling B. 2011. Model for membrane organization and protein sorting in the cyanobacterium Synechocystis sp. PCC 6803 inferred from proteomics and multivariate sequence analyses. J Proteome Res 10:3617–31.

69. Mustardy L, Los DA, Gombos Z, Murata N. 1996. Immunocytochemical localization of acyl-lipid desaturases in cyanobacterial cells: evidence that both thylakoid membranes and cytoplasmic membranes are sites of lipid desaturation. Proc Natl Acad Sci U S A 93:10524–7.

70. Singh SC, Sinha RP, Häder D. 2002. Role of Lipids and Fatty Acids in Stress Tolerance in

Cyanobacteria. Acta Protozool 41:297–308.

71. Mullineaux CW. 2014. Electron transport and light-harvesting switches in cyanobacteria. Front Plant Sci 5:1–6.

72. Liu L-N. 2015. Distribution and dynamics of electron transport complexes in cyanobacterial thylakoid membranes. Biochim Biophys Acta - Bioenerg.

73. Klementiev KE, Tsoraev G V, Tyutyaev E V, Zorina AA, Feduraev P V, Allakhverdiev SI, Paschenko VZ. 2017. Membrane fluidity controls redox-regulated cold stress responses in cyanobacteria. Photosynth Res 0:0.

74. Mackey KRM, Paytan A, Caldeira K, Grossman AR, Moran D, McIlvin M, Saito MA. 2013. Effect of temperature on photosynthesis and growth in marine Synechococcus spp. Plant Physiol 163:815–29.

75. Mao H Bin, Li GF, Ruan X, Wu QY, Gong YD, Zhang XF, Zhao NM. 2002. The redox state of plastoquinone pool regulates state transitions via cytochrome b6f complex in Synechocystis sp. PCC 6803. FEBS Lett 519:82–86.

76. El Bissati K, Delphin E, Murata N, Etienne a, Kirilovsky D. 2000. Photosystem II fluorescence quenching in the cyanobacterium Synechocystis PCC 6803: involvement of two different mechanisms. Biochim Biophys Acta 1457:229–242.

77. Ajlani G, Kirilovsky D, Picaud M, Astier C. 1989. Molecular analysis of psbA mutations responsible for various herbicide resistance phenotypes in Synechocystis 6714. Plant Mol Biol 13:469–79.

78. Lee TX, Metzger SU, Cho YS, Whitmarsh J, Kallas T. 2001. Modification of inhibitor binding sites in the cytochrome bf complex by directed mutagenesis of cytochrome b6 in Synechococcus sp. PCC 7002. Biochim Biophys Acta - Bioenerg 1504:235–247.

79. Gombos Z, Wada H, Murata N. 1994. The recovery of photosynthesis from low-temperature photoinhibition is accelerated by the unsaturation of membrane lipids: a mechanism of chilling tolerance. Proc Natl Acad Sci U S A 91:8787–91.

5

LEGENDS

Figure 1. Flow diagram and nutrient streams obtained from the Nine Springs Wastewater Treatment Plant (Dane County, Wisconsin, USA). Stars indicate sampling points.

Figure 2. Excitation Emission Matrix of (A) Medium A+, (B) Secondary Effluent, (C) 6.25% GBF, and (D) 12.5% GBF. Fluorescence values were normalized to 1 ppm of quinine sulfate in 0.1 N H_2SO_4 at Ex/Em = 350/450 nm.

Figure 3. Biomass accumulation for cultures grown in Medium A^+, 6.25 %, 9.9 %, or 12.5 % (v/v) GBF media with 1 % CO_2 at (A) 37°C and 200 μmol photons m^{-2} s^{-1}, (B) 37°C and 100 μmol photons m^{-2} s^{-1}, (C) 27°C and 200 μmol photons m^{-2} s^{-1}, or (D) 27°C and 100 μmol photons m^{-2} s^{-1}. The values represent the mean ± SD of biological triplicates.

Figure 4. Membrane permeability of cultures grown in Medium A^+, 6.25 %, 9.9 %, or 12.5 % (v/v) GBF media with 1 % CO_2 at (A) 37°C and 200 μmol photons m^{-2} s^{-1}, (B) 37°C and 100 μmol photons m^{-2} s^{-1}, (C) 27°C and 200 μmol photons m^{-2} s^{-1}, or (D) 27°C and 100 μmol photons m^{-2} s^{-1}. The values represent the mean ± SD of biological triplicates.

Figure 5. Reactive oxygen species and membrane permeability assay. Cells were grown to early linear phase in Medium A^+ or 12.5% GBF with the appropriate treatment under continuous illumination (200 μmol photons m^{-2} s^{-1}) with 1 % CO_2 at 37°C. Fluorescence values were normalized to $OD_{730.}$ The values represent the mean ± SD of biological triplicates.

Figure 6. Absorption spectra of PCC 7002 cultures exposed to GBF, at two different cultivation temperatures. Cultures were grown in Medium A^+, 6.25 %, or 12.5 % (v/v) GBF media under continuous illumination (200 μmol photons m^{-2} s^{-1}) with 1 % CO_2 at (A) 37°C or (B) 27°C for 72

hours. The spectra were recorded in dilute cell suspensions and normalized to an OD_{730}. The peak at 438 nm is due to carotenoids, the peak at 637 nm is due to phycobilisomes, and the peak at 683 nm is due to chlorophyll a.

Figure 7. Rates of oxygen evolution as a function of acclimation temperature and light intensity. Cells were grown to early linear phase in Medium A^+ or 12.5% GBF under continuous illumination (200 μmol photons m^{-2} s^{-1}) with 1 % CO_2 at (A) 37°C or (B) 27°C. Cells were pelleted, resuspended in Medium A^+ or 12.5% GBF, and the rate of maximal oxygen evolution was measured with 10 mM HCO_3^- as an electron acceptor at increasing light intensities. The values represent the mean ± SE of biological duplicates.

Figure 8. Photosynthetic oxygen evolution rates at saturating light conditions. Cells were grown to early linear phase in Medium A^+ under continuous illumination (200 μmol photons m^{-2} s^{-1}) with 1 % CO_2 at 37°C). Cells were pelleted and resuspended in Medium A^+, 12.5% GBF, 12.5% GBF + 310 mM NaCl (control for osmolarity), 12.5% GBF prefiltered with activated carbon, Medium A^+ + 10 μM DCMU (control for inhibition for electron transport), or pre-treated with 800 μg ml^{-1} Lincomycin for 1 hour (control for the inhibition of protein synthesis.) Maximal oxygen evolution rates were measured with 10 mM HCO_3 as an electron acceptor at 2700 μmol photons m^{-2} s^{-1}. The values represent the mean ± SE of biological duplicates.

TABLES

Table 1. Nutrient composition of batch of 100% GBF used for subsequent experiments

Analyte[a]	Concentration[b] (mg L^{-1}) (±SD)
NH_3–N	1180 ± 135
NO_3–N	7.5 ± 0.04
SRP	78 ± 10
COD	735 ± 4
TSS	467 ± 123
VSS	18 ± 2
TS	2350 ± 36
TS (Glass Fiber Filtered)	2030 ± 42
TS (0.45 um membrane filtered)	2000 ± 151

[a] SRP-soluble reactive phosphorus, COD-chemical oxygen demand, TSS- total suspended solids, VSS – volatile suspended solids, TS-total solids

[b] Values shown represent the mean ± standard deviation (SD) of at least three technical replicates.

Table 2. Characteristics of GBF and secondary effluent over the 6 month experimental period.

Source	Analyte	Concentration[a] (mg L^{-1}) (±COV)
GBF	NH_3–N	920 ± 22%
	NO_3–N	3.9 ± 43%
	SRP	54 ± 27%
Secondary Effluent	NH_3–N	n.d.
	NO_3–N	19.3 ± 6.6%
	SRP	n.d.

[a] Values shown represent the mean ± coefficient of variation (COV) of at least three technical replicates.

Table 3. Growth Rates with varying Temperature and Light Intensity

Media	Light Intensity (µmol photons m^{-2} s^{-1})	Temperature (°C)	Growth Rate (±SD) (OD day^{-1})
A^+	200	37	0.66 ± 0.04
6.25% GBF	200	37	0.58 ± 0.05
12.5% GBF	200	37	0.05 ± 0.01
A^+	100	37	0.28 ± 0.01
6.25% GBF	100	37	0.24 ± 0.01
9.9% GBF	100	37	0.11 ± 0.02
12.5% GBF	100	37	0.02 ± 0.00
A^+	200	27	0.73 ± 0.08
6.25% GBF	200	27	0.32 ± 0.03
9.9% GBF	200	27	0.42 ± 0.06
12.5% GBF	200	27	0.28 ± 0.04
A^+	100	27	0.25 ± 0.01
6.25% GBF	100	27	0.26 ± 0.02
9.9% GBF	100	27	0.24 ± 0.01
12.5% GBF	100	27	0.26 ± 0.02

[a] Linear growth rates of cultures grown in Medium A^+ or GBF with the appropriate treatment under continuous illumination (200 µmol photons m^{-2} s^{-1} or 100 µmol photons m^{-2} s^{-1}) with 1 % CO_2 at 37°C or 27°C. The values represent the mean ± SD of biological triplicates.

Table 4. Fatty acid content and composition of cultures grown in Medium A^+ or 12.5% GBF media under continuous illumination (200 μmol photons m^{-2} s^{-1}) at 27°C for 72 hours

Growth Conditions[1]		Fatty Acids Species					
		C16:0	C16:1 Δ9	C18:0	C18:1 Δ9	C18:2 Δ9,12	C18:3 Δ9,12,15
Medium A^+	mg FA $gDCW^{-1}$	6.7 ± 0.7	2.0 ± 0.1	0.2 ± 0.1	1.5 ± 0.2	3.3 ± 0.2	1.4 ± 0.1
	% FA	44 ± 1	13 ± 1	2 ± 0	10 ± 0	22 ± 1	9 ± 1
GBF	mg FA $gDCW^{-1}$	11.6 ± 3.1	3.5 ± 0.8	1.3 ± 0.3	2.2 ± 0.7	3.9 ± 0.8	4.4 ± 1.6
	% FA	43 ± 0	13 ± 0	5 ± 0*	8 ± 0	15 ± 1*	16 ± 1*

[1] Strains were grown in the Medium A^+ or 12.5% GBF media under continuous illumination (200 μmol photons m^{-2} s^{-1}) at 27°C for 72 hours. Fatty acids were extracted and derivatized as previously described. The values represent the mean ± SD of two independent experiments. * represent statistically significant differences from control (p-value<0.005 using an unpaired t-test)

S

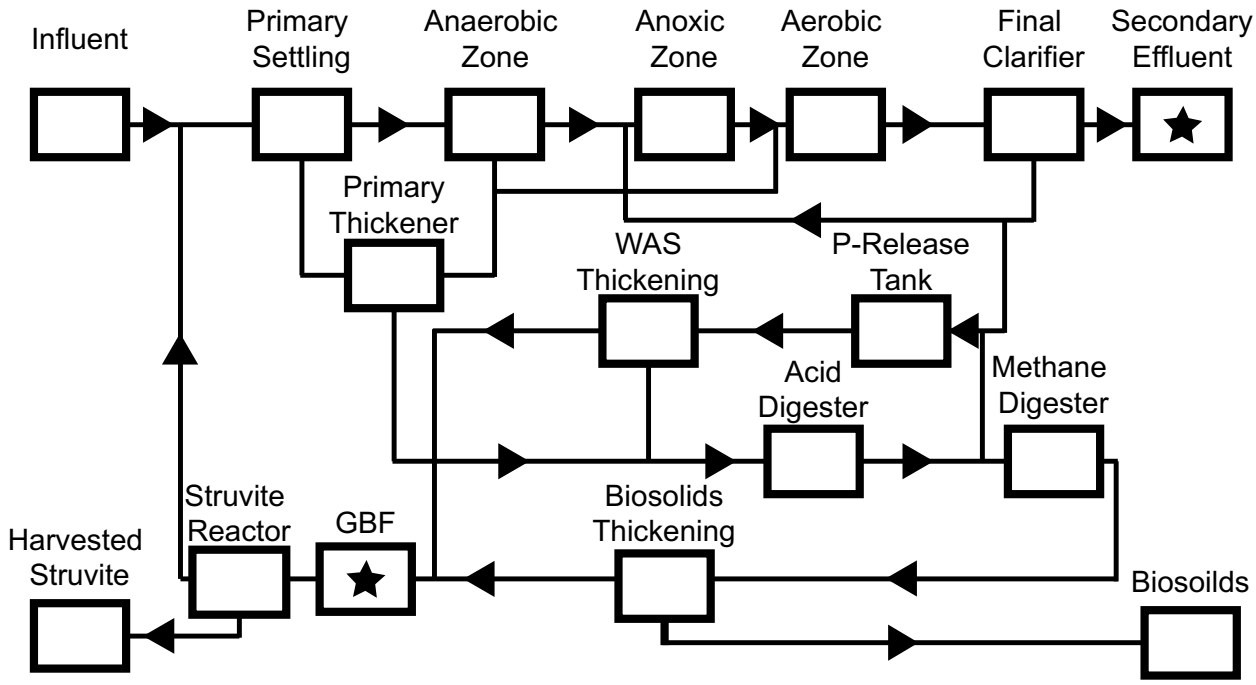

Figure 1. Flow diagram and nutrient streams obtained from the Nine Springs Wastewater Treatment Plant (Dane County, Wisconsin, USA). Stars indicate sampling points.

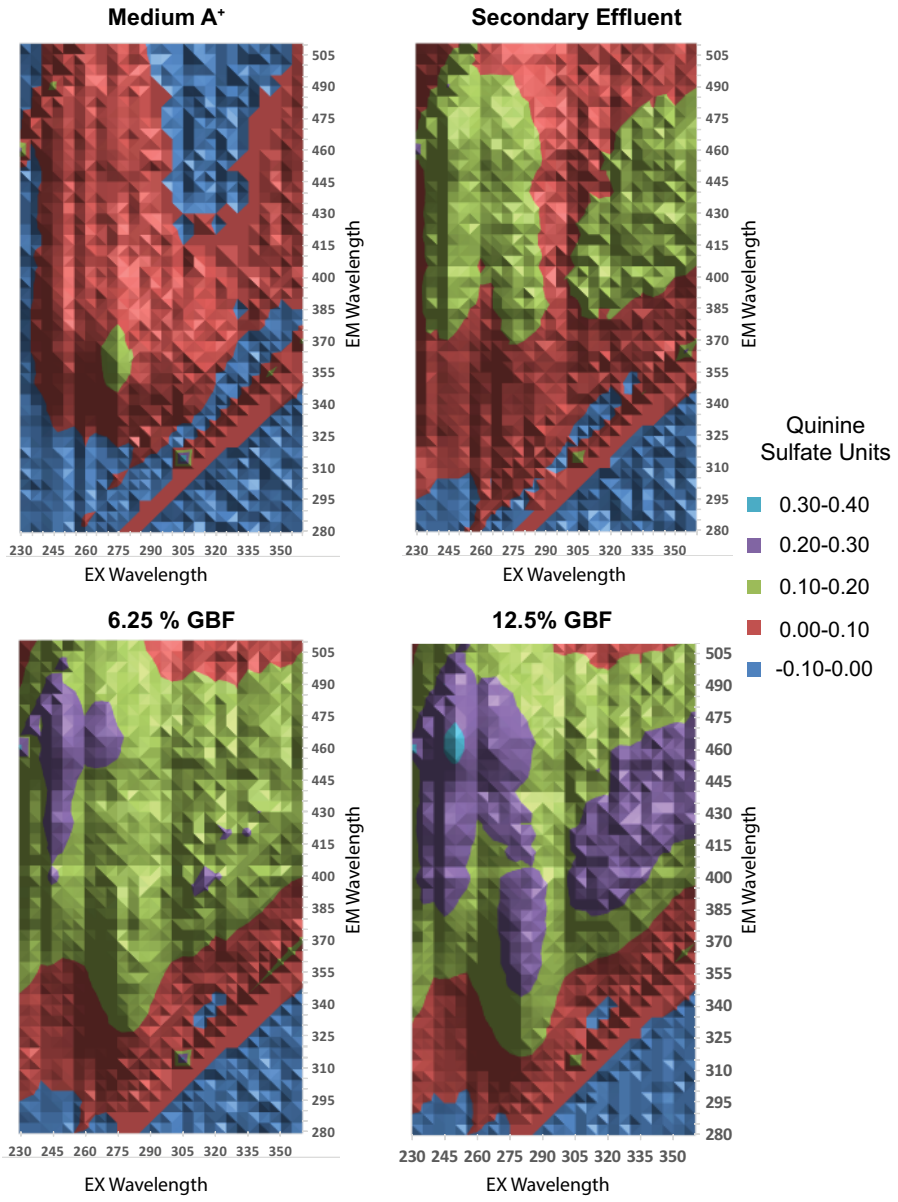

Figure 2. Excitation Emission Matrix of (A) Medium A^+, (B) Secondary Effluent, (C) 6.25% GBF, and (D) 12.5% GBF. Fluorescence values were normalized to 1 ppm of quinine sulfate in 0.1 N H_2SO_4 at Ex/Em = 350/450 nm.

5

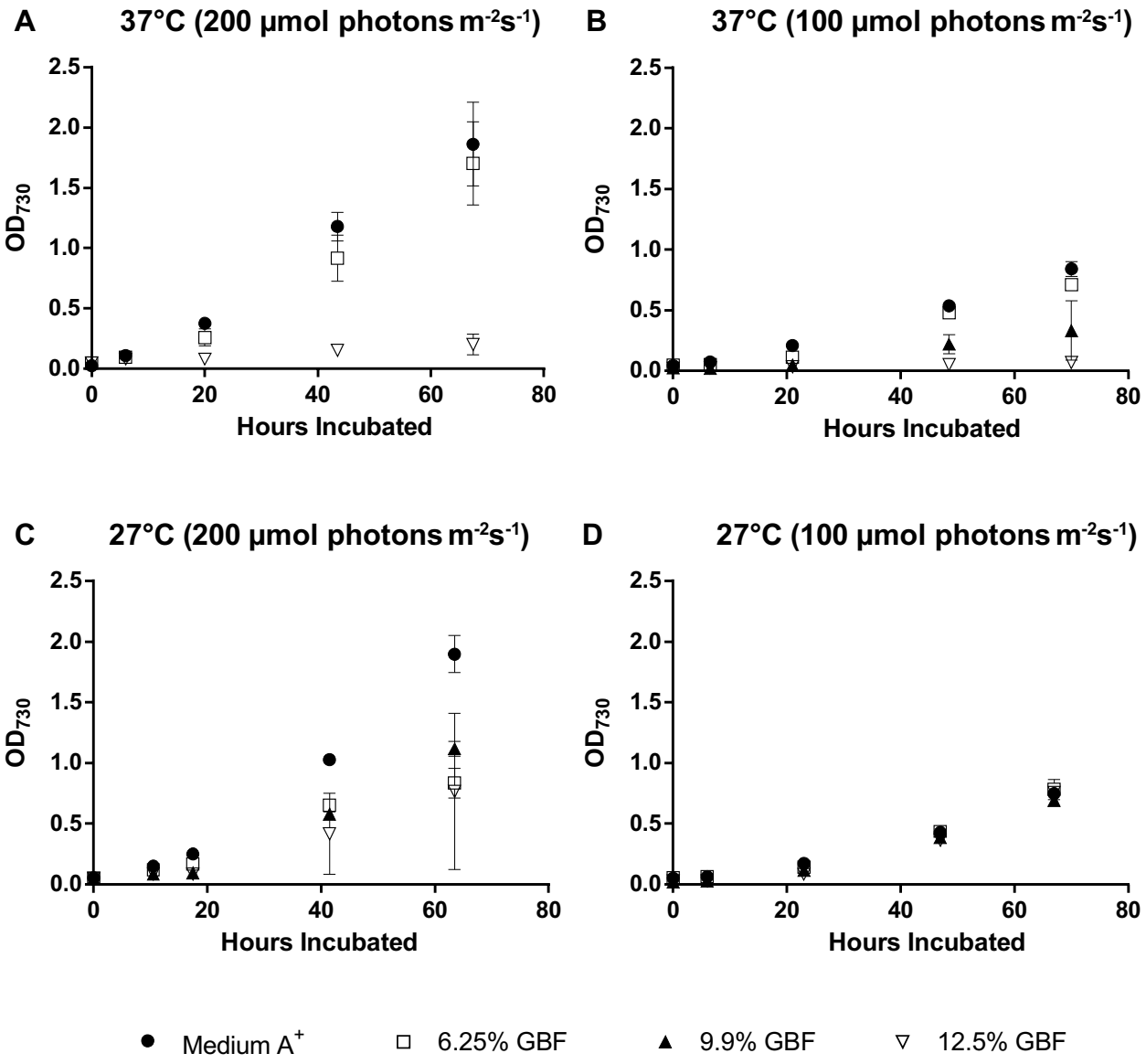

Figure 3. Biomass accumulation for cultures grown in Medium A^+, 6.25 %, 9.9 %, or 12.5 % (v/v) GBF media with 1 % CO_2 at (A) 37°C and 200 µmol photons m^{-2} s^{-1}, (B) 37°C and 100 µmol photons m^{-2} s^{-1}, (C) 27°C and 200 µmol photons m^{-2} s^{-1}, or (D) 27°C and 100 µmol photons m^{-2} s^{-1}. The values represent the mean ± SD of biological triplicates.

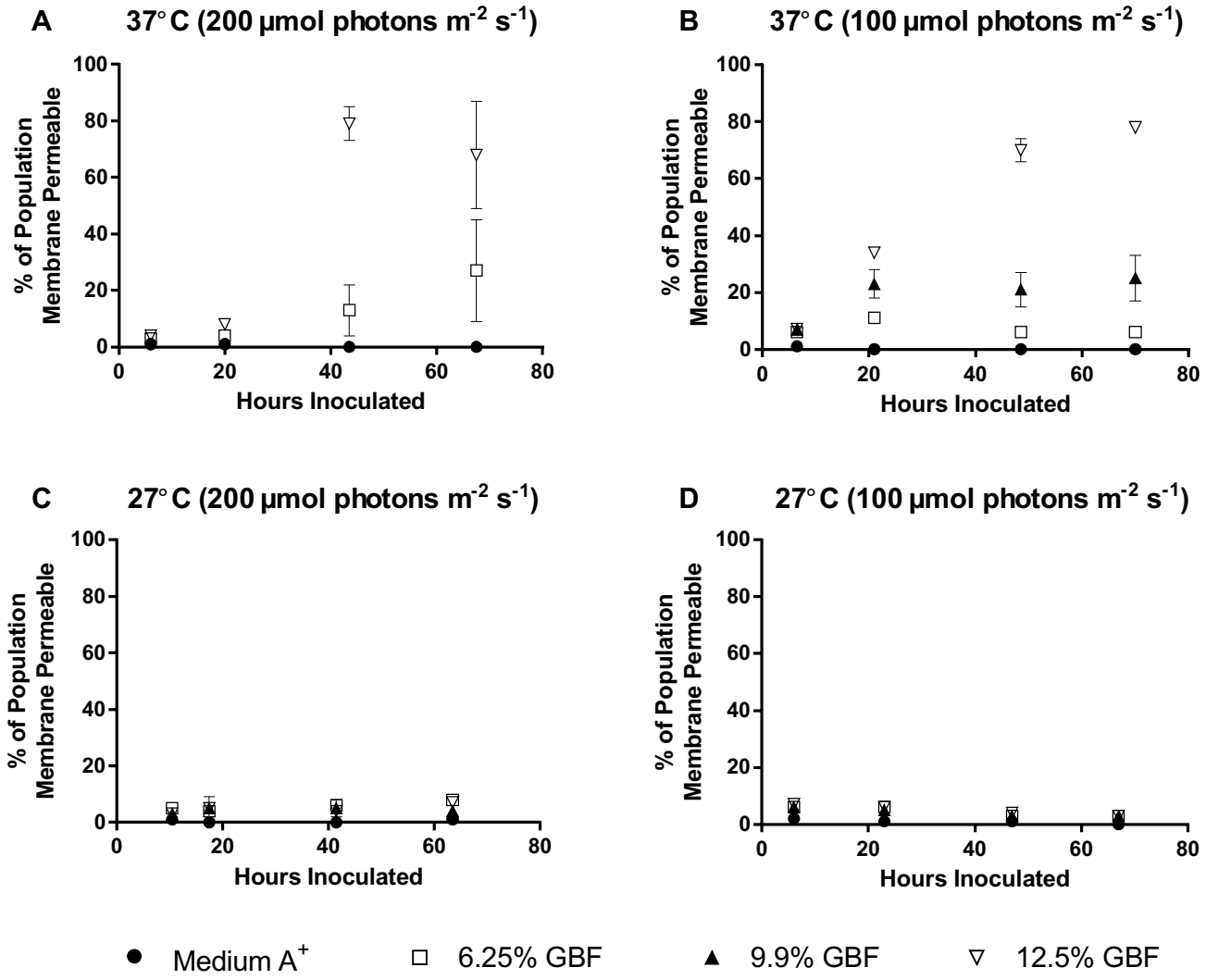

Figure 4. Membrane permeability of cultures grown in Medium A^+, 6.25 %, 9.9 %, or 12.5 % (v/v) GBF media with 1 % CO_2 at (A) 37°C and 200 µmol photons m^{-2} s^{-1}, (B) 37°C and 100 µmol photons m^{-2} s^{-1}, (C) 27°C and 200 µmol photons m^{-2} s^{-1}, or (D) 27°C and 100 µmol photons m^{-2} s^{-1}. The values represent the mean ± SD of biological triplicates.

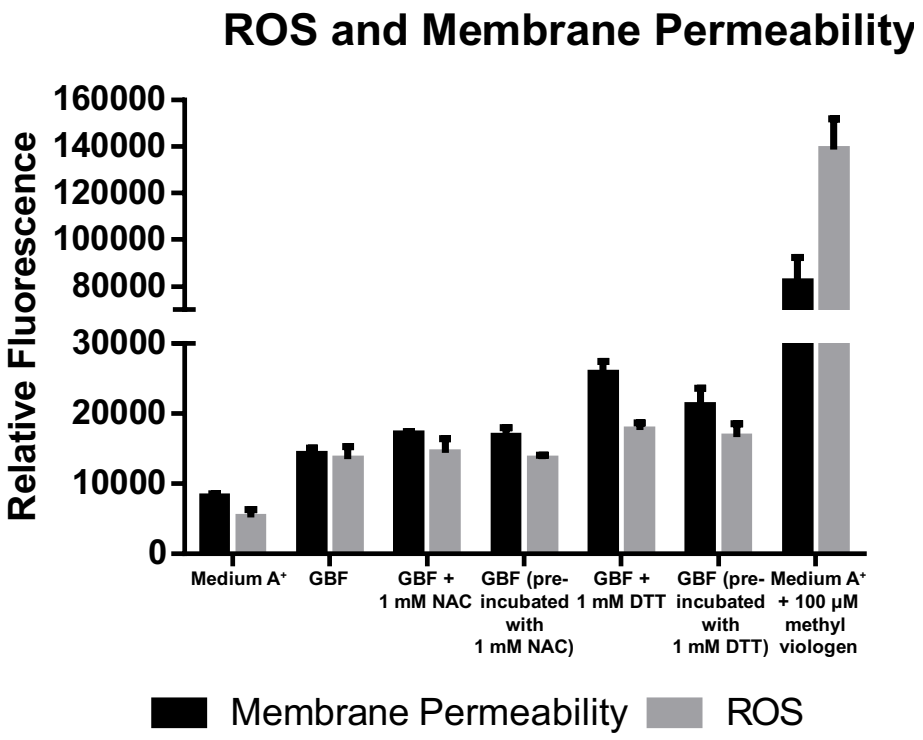

Figure 5. Reactive oxygen species and membrane permeability assay. Cells were grown to early linear phase in Medium A^+ or 12.5% GBF with the appropriate treatment under continuous illumination (200 µmol photons m^{-2} s^{-1}) with 1 % CO_2 at 37°C. Fluorescence values were normalized to OD_{730}. The values represent the mean ± SD of biological triplicates.

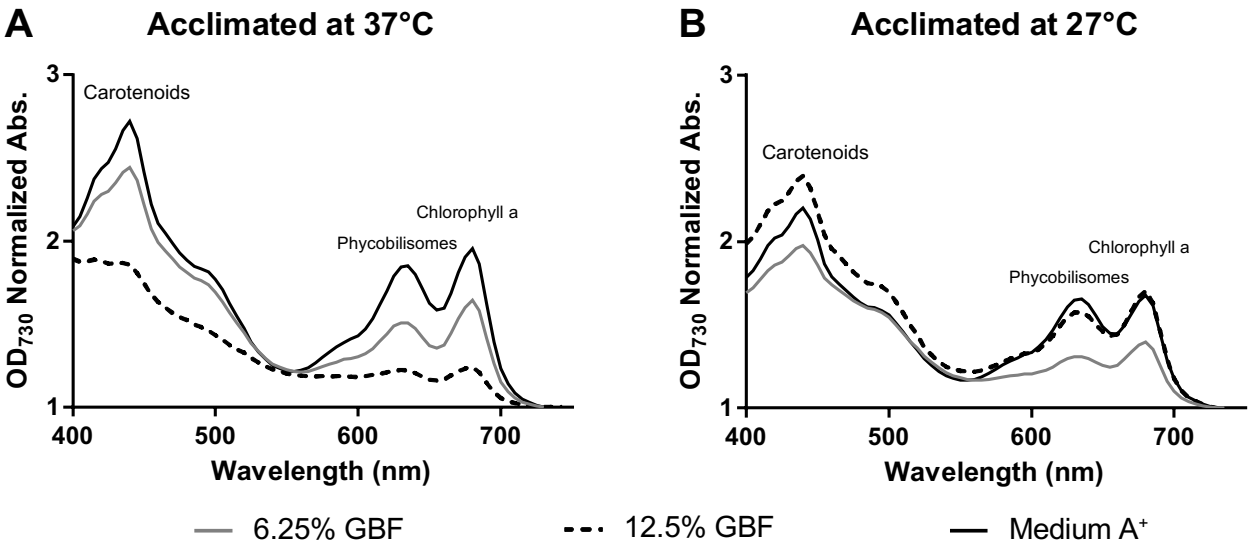

Figure 6. Absorption spectra of PCC 7002 cultures exposed to GBF, at two different cultivation temperatures. Cultures were grown in Medium A^+, 6.25 %, or 12.5 % (v/v) GBF media under continuous illumination (200 µmol photons m^{-2} s^{-1}) with 1 % CO_2 at (A) 37°C or (B) 27°C for 72 hours. The spectra were recorded in dilute cell suspensions and normalized to an OD_{730}. The peak at 438 nm is due to carotenoids, the peak at 637 nm is due to phycobilisomes, and the peak at 683 nm is due to chlorophyll a.

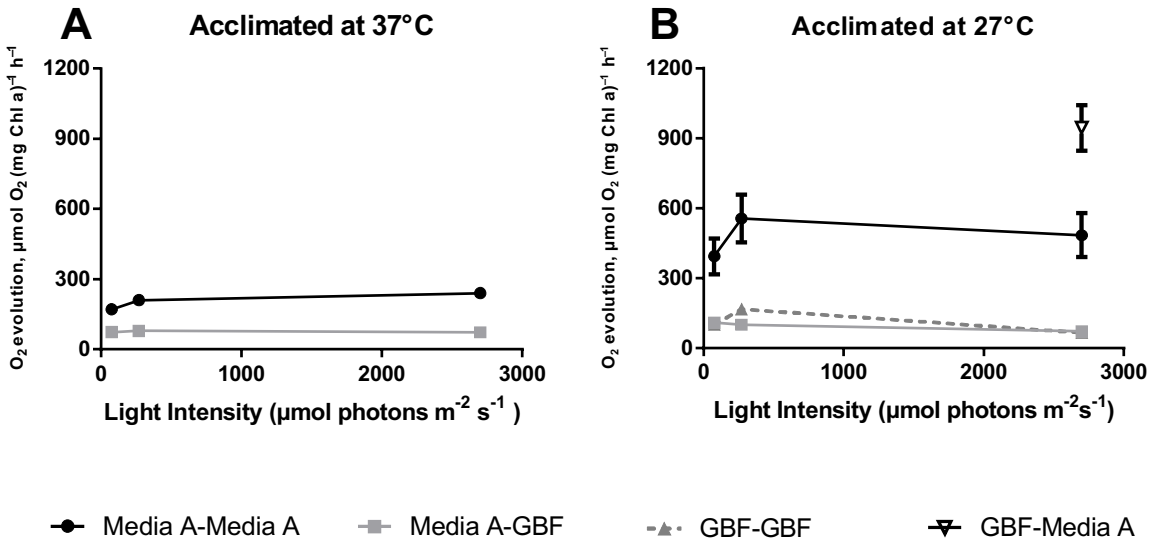

Figure 7. Rates of oxygen evolution as a function of acclimation temperature and light intensity. Cells were grown to early linear phase in Medium A^+ or 12.5% GBF under continuous illumination (200 µmol photons m^{-2} s^{-1}) with 1 % CO_2 at (A) 37°C or (B) 27°C. Cells were pelleted, resuspended in Medium A^+ or 12.5% GBF, and the rate of maximal oxygen evolution was measured with 10 mM HCO_3^- as an electron acceptor at increasing light intensities. The values represent the mean ± SE of biological duplicates.

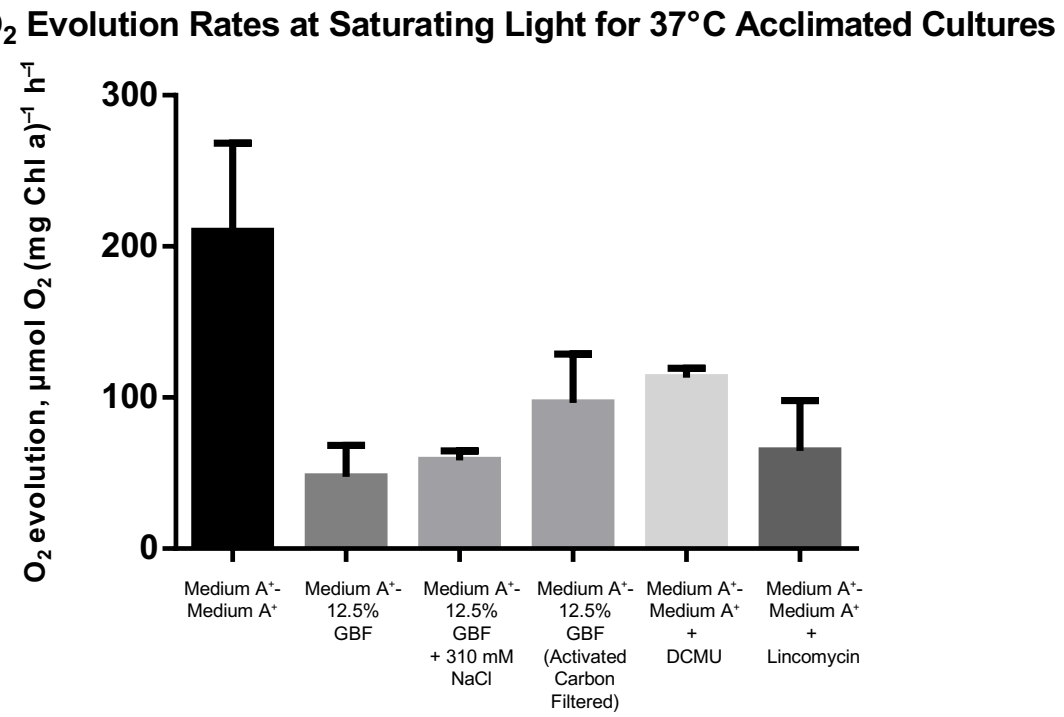

Figure 8. Photosynthetic oxygen evolution rates at saturating light conditions. Cells were grown to early linear phase in Medium A^+ under continuous illumination (200 µmol photons m^{-2} s^{-1}) with 1 % CO_2 at 37°C). Cells were pelleted and resuspended in Medium A^+, 12.5% GBF, 12.5% GBF + 310 mM NaCl (control for osmolarity), 12.5% GBF prefiltered with activated carbon, Medium A^+ + 10 µM DCMU (control for inhibition for electron transport), or pre-treated with 800 µg ml^{-1} Lincomycin for 1 hour (control for the inhibition of protein synthesis.) Maximal oxygen evolution rates were measured with 10 mM HCO_3 as an electron acceptor at 2700 µmol photons m^{-2} s^{-1}. The values represent the mean ± SE of biological duplicates.